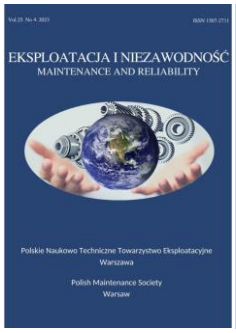

Eksploatacja i Niezawodnosc – Maintenance and Reliability
Volume 25 (2023), Issue 4
journal homepage: http://www.ein.org.pl

Article citation info:
Czyż Z, Jakubczak P, Podolak P, Skiba K, Karpiński P, Droździel-Jurkiewicz M, Wendeker M, Deformation measurement system for UAV components to improve their safe operation, Eksploatacja i Niezawodnosc – Maintenance and Reliability 2023: 25(4) http://doi.org/10.17531/ein/172358

Deformation measurement system for UAV components to improve their safe operation

Indexed by:
Web of Science Group

Zbigniew Czyż[a,*], Patryk Jakubczak[b], Piotr Podolak[b], Krzysztof Skiba[c], Paweł Karpiński[d], Magda Droździel-Jurkiewicz[b], Mirosław Wendeker[c]

[a] Aeronautics Faculty, Polish Air Force University, Poland
[b] Department of Materials Engineering, Faculty of Mechanical Engineering, Lublin University of Technology, Poland
[c] Department of Thermodynamics, Fluid Mechanics and Aviation Propulsion Systems, Lublin University of Technology, Poland
[d] Department of Machine Operation and Production Process Management, Faculty of Production Engineering, University of Life Sciences in Lublin, Poland

Highlights

- The method allows the analysis of CFRP fuselage deformation for UAV design.
- Effective PID control algorithm and stand simulate flight operations.
- DIC system enables precise displacement and deformation analysis of specific points in the structure.
- Method enables effective UAV deformation analysis and design optimization for enhanced safety.

Abstract

The paper presents the authors' method and test rig for performing the deformation analysis of unmanned aircraft fuselages. To conduct the analysis, the DIC system was used, as well as a test rig designed and constructed by the authors, equipped with a dedicated control and load control system. The article presents a description of the research capabilities of the test rig developed for testing the deformation of unmanned aircraft fuselages. Due to the specific operating conditions of the designed fuselage, the test rig developed allows the simulation of loads corresponding to different flight conditions. In addition, it is possible to change the forces acting on the fuselage simultaneously for all servos or each of them separately. Finally, results showing the displacement of component control points for the considered fuselage versions are presented. The tests carried out using the developed test rig allowed the verification of the maximum deformations. The two versions of the composite fuselage of an aerial vehicle have been compared in the paper. The created measurement system and performed analyzes have enabled us to identify and quantitatively analyze the weaknesses of the construction. The results have enabled us to geometrically modify the construction so the mass of the fuselage reduced by 19% and a coefficient of construction balance increased by 22%.

Keywords
strength tests, deformation measurement, optical displacement and deformation analysis, digital image correlation, UAV

1. Introduction

Fibrous composites are widely used in aircraft construction [9]. Their good strength properties, combined with the ease of shaping the structure of the designed object make them widely used, not only for the construction of light unmanned aerial vehicles, but also for large passenger aircraft. A review of recent advances using composites in modern aircraft construction was presented by Soutis (2005) [26]. Polymer composites [15] and layered structures that are a combination of metal alloy and

(*) Corresponding author.
E-mail addresses: Z. Czyż (ORCID: 0000-0003-2281-1149) z.czyz@law.mil.pl, P. Jakubczak (ORCID: 0000-0003-3770-571X) p.jakubczak@pollub.pl, P. Podolak (ORCID: 0000-0002-4042-9966) p.podolak@pollub.pl, K. Skiba (ORCID: 0000-0001-5504-3946) k.skiba@pollub.pl, P. Karpiński (ORCID: 0000-0001-5786-1248) pawel.karpinski@up.lublin.pl, M. Droździel-Jurkiewicz (ORCID: 0000-0003-2756-5960) m.drozdziel@pollub.pl, M. Wendeker (ORCID: 0000-0003-4121-8818) m.wendeker@pollub.pl

fibre/epoxy prepreg are also used in aviation [30]. However, in the case of aircraft structures, it is particularly important to assess fatigue crack growth rate and crack detection rate for risk evaluation [32].

Studies of the strength of the composite structure of an aircraft fuselage or its components can be conducted both experimentally and numerically. For numerical analysis, a commonly used method is the finite element method (FEM) [14]. This paper [5] presents an example of the use of this method and presents an analysis of the strength of composite flexible landing-gear legs. Experimental strength testing involves applying loads to the structure under test at selected locations and measuring its displacements and deformations. For this purpose, strain gauges pasted on the surface of the test object are often used [17]. This paper [27] presents dynamic tests of aircraft structures and the validation of the presented procedure on a selected structure. Among the strength tests, we can also distinguish fatigue tests, which make it possible to assess the strength of a given object subjected to cyclic loading [29]. Another method that is becoming increasingly popular for testing aerospace structures is the optical technique based on the Aramis system [21]. This technique consists of the optical observation of defined points on the surface of the structure under test and the digital processing of the recorded images under various loading conditions. In general, the studies can also consider the effects of fatigue loads and effects of natural aging on the residual strength of the composite structure [11].

Baqersad [2] has presented an overview of various photogrammetry techniques, such as point tracking and digital image correlation. One such method is digital image correlation (DIC). It is a non-contact optical method that allows the analysis of vibrations and loads on structures. A high-contrast speckle pattern structure is applied to the tested surface. A series of images are then taken using cameras. The DIC method works by creating overlapping fields in the area under study. The size of the field ranges from a dozen to a few dozen square pixels. A given field usually contains several pixels of the applied pattern. The random distribution of spot patterns makes each field have its own value of reflectance and absorption of light intensity. This allows an algorithm in the software to recognize the motion of each field and convert it into the displacement and deformation of the surface under study [2]. The advantage of this method is that no load is induced on the structure under test, compared to measurement methods using accelerometers. This method was presented by Patil et al. in their work [23], in which a pair of high-speed cameras was used to measure the dynamic response of a fender structure. Excitation was implemented in the form of a force set using an impact hammer. The proposed approach made it possible to obtain the modal shapes of the complex structure using this optical technique. Another example, in which the DIC method was used to determine the form of deformation of the studied structure (membrane), is the work of Bleischwitz et al. [4]. Digital image correlation can provide an auxiliary measurement method for standard strain gauge measurement. Gradl [13] used this technique to supplement the data provided by traditional strain gauges in large-scale rocket engine testing. This is because strain gauges are prone to detachment at elevated temperatures and are limited to local measurements.

The DIC technique was also used to obtain vibration characteristics of wind turbine blades, which can be used to monitor the structural condition of such structures. [18] A stereo camera system that was installed on a drone was used to record blade deflections. This technique makes it possible to remotely monitor the condition of wind turbines located both onshore and offshore. An interesting use of the Image Pattern Correlation Technique (IPCT) based on DIC is presented in the work of Stasicki and Boden [28]. It used a system of two digital cameras placed on a surveyed aircraft propeller. This enabled the non-invasive in-flight measurement of propeller deformation. In turn, in a study conducted by Littell [20], the digital image correlation method was used to analyse airframe deformation during ongoing crash tests.

Studying the motion and deformation of high-speed rotating machinery is a major engineering challenge. Ye et al. [31] presented a method for image acquisition of a rotor rotating at high speed using a low-speed camera with 3D digital image correlation. The method used allows the low-speed camera to acquire images of the entire circle asynchronously while the blades are rotating rapidly. Compared to methods using a high-speed camera, the proposed method has a lower cost and a high flexibility of measurement resolution. A layer-by-layer matching method is proposed for finding points between two rotated images. Meanwhile, a binocular rotation correlation

method was used to correlate subsets of spots.

The DIC method is also used in the study of large-scale composite structures. An analysis by Janeliukstis [16] showed that the technique is particularly applicable in the wind power and aerospace sectors. It is used to measure displacements and deformations under static loading and operational modal analysis in dynamic structural studies. An example of this approach is presented in the paper [7], in which damage growth in a composite wind-turbine blade under fatigue loading was experimentally studied. The DIC technique was used to quantify the buckle wave of the trailing edge. The same method was used by Gardner [12] when studying the buckling of a cylindrical shell structure and by Balac [1] to determine the critical areas for crack initiation on the pressure vessel structure.

Composite structures (especially in aviation applications) are examined by means of non-destructive techniques (NDT), including the most popular ones like ultrasonic and radiographic techniques. These techniques enable us to detect different types of defects, e.g. discontinuity, delamination or porosity in materials. A radiographic technique is applied in sandwich structures with a metal honey comb core. NDTs are developing and new techniques like coplanar capacitive sensors (CCS) [22] or mechanoluminescence (ML) combined with digital image correlation (DIC) [25] have emerged

This research is based on experiments to guarantee a safe usage of the created composite structure during further flight testing. Consequently, a special deformation measurement system for UAVs was created. The geometry of the created fuselage and its tail is highly complex, which requires a highly advanced technology of manufacturing. Such a technology involves irregular overlapping layers and technologically fragmented layers that finally have an impact on strength characteristics. The FEM approach means creating a model that has evenly distributed fabrics and no real defects of lamination of a composite structure are assumed. Experimental results are to verify FEM analyses and further calibrate numerical models. The final fuselage structure is so technologically complex that its final strength verification can be experimental only, including full-scaled stand and flight testing. Besides the evaluation how the structure behaves under loading in real time and what its load capacity is, experimental validation is an incredibly valuable source of knowledge how to further improve and calibrate numerical models created in earlier stages of a proof of concept.

The measurement system presented in this paper for the deformation analysis of structures made of CFRP (Carbon Fibre Reinforced Polymer), dedicated to unmanned aerial vehicles, is a combination of the digital image correlation (DIC) method with a proprietary subsystem for specifying and controlling the loading of the components of the tested structure. It was developed for the implementation of a scientific project and was adapted to the unique design of the aircraft. The stand itself allows the time-controlled setting of the values of the forces that load the object, with the help of seven servos operating together with the same force value or each with a different one, depending on the needs. In addition, unlike other systems in use, it is possible to easily change the configuration and location of force application points.

The construction of the UAV presented in this paper stands out from concepts of aerial vehicles so far developed due to its innovative propulsion system. Thus, verification of the construction's strength requires an unconventional approach. The authors believe that the above-mentioned combination of a DIC system, original test rig, force-control algorithm and a way of data post-processing is crucial for the future investigation of such objects and scientific studies connected to them, due to its versatility and easiness of load case generation, both for static and dynamic response (mainly fatigue).

One of the more common methods for evaluating strength and deformations of complex structures under complex loading conditions is the finite element method (FEM). However, the use of the FEM method is fraught with uncertainty if researching into complex composite structures whose manufacturing process involves forced technological treatments such as irregular overlapping layers, intersection of layers, local reinforcements and structural defects themselves. Numerical models do not reflect such aspects so can be successfully used for conceptual work and preliminary validation, but due to the above limitations, the FEM method cannot replace experimental methods in implementation stages of aerial vehicles. The proposed measurement method, however, has the advantage of providing data on deformations over the full spectrum of loads in full-scale tests on any surface. In addition, FEM simulations require a researcher to be experienced to correctly interpret

results and are sensitive to boundary conditions, including mesh simplifications at locations with complex geometries. The accuracy of the finite element method also depends on an input of material data that actually reflect averaged values of normalized samples, which in composite structures is of great importance due to different manufacturing technologies, layer formation precision, etc. The computational time for complex geometric models can be long so to shorten it, access to a high-powered computing cluster may be necessary. Testing the structure on a testing machine also has drawbacks, e.g. limitations due to measuring complex loading conditions. This type of equipment is generally designed to test composites under simple loading conditions such as tension, bending and compression. This fact indirectly affects measurement accuracy in the case of complex stress conditions. Moreover, this is a destructive method that leads to irreversible damage to tested structures. Other non-destructive techniques that allow us to test composites are ultrasonic or radiographic testing, but such techniques enable us to detect cracks, delamination and discontinuities in composites rather than measure deformation (displacement) of materials.

The measurement system proposed in this paper eliminates the aforementioned drawbacks and allows measuring a real deformation of the entire composite structure. It enables us to research regardless of object shapes and applied loads. This method does not necessarily lead to damage to the structure (it depends on the magnitude of the applied loads). The measurement procedure is fast and does not require long and computationally intensive calculations.

The main objective of this paper is to present the principles of this measurement technique's operation and to prove its versatility by demonstrating a set of various load cases expected to occur during the UAV's work and analysing their effect on the aircraft's response. As a secondary objective, the authors stated a demonstration of how collected measurements may be exploited to improve the construction of the considered UAV.

2. RESEARCH OBJECT

The UAV fuselage deformation test bench developed is dedicated to a hybrid UAV, characterized by the increased functionality resulting from the combination of the advantages of a gyrocopter and a multicopter. The classical propulsion system of a gyrocopter will be supported by additional electric motors with propellers and adjustable thrust vectoring. This propulsion system will be used for reasons of flight safety and the optimal management of the power required for flight. Multi-rotor aircraft are becoming increasingly popular. They are characterized by relatively high energy consumption during flight involving hovering. The XGyro multi-rotor aircraft propulsion system will enable vertical take-off. When the required forward speed is reached under the influence of the flowing air, the auto-rotating main rotor starts generating lift force. The redundant lift-generating propulsion system increases landing safety. Due to the possible different landing techniques and the two independent lift-generating propulsion systems, the XGyro aircraft is safer than the competing solutions. The actual progressive flight is performed using autorotation due to the lower energy requirements. Such a system requires, among other things, the use of a sufficient number of actuators on the bench to set the load at a certain value. The complete research object is shown in Fig. 1. XGyro is an unmanned aerial vehicle with an MTOW of 5 kg and the diameter of the main rotor equals 2 m.

Fig. 1. View of the XGyro visualization (left) and real object (right).

A presentation of the test object is justified at this stage before presenting the developed test bench. The entire fuselage of the aircraft was made of CFRP fabric (Fig. 2). It is the first version, which was analysed to verify its correct manufacturing. Before strength tests are carried out, it is very important to verify the composite structure's correctness. Even as a result of macroscopic observations it is possible to identify possible defects, such as surface defects, inclusions on the composite surface, geometric mistakes, layer irregularities, expositions of carbon fibres, or areas of poor-quality adhesive joints. This is important because possible defects may affect the strength of the tested object during the strength tests. In extreme conditions, it may lead to its destruction.

Fig. 2. View of the first version of the UAV fuselage as prepared for strength tests.

To show the possibility of using the system developed to optimize the structure, two objects were considered for analysis. While Fig. 2 shows the first version of the structure developed, Fig. 3 shows the object representing the second version. By analysing the results, structures with better strength properties were obtained. A detailed analysis will be the subject of consideration in later sections of this article.

Fig. 3. View of the second version of the UAV fuselage prepared for strength tests.

The first version of the test object (Version I) was made entirely of four layers of CFRP fabric. The second test object (Version II), on the other hand, used the same CFRP fabric but applied a reduction of layers in areas that did not show

significant deformation. The entire structure of both models was manufactured using carbon/epoxy composites based on a prepreg technology. The thermoset epoxy resin M79 (Hexcel, USA) was used as the matrix, while the fibers were 3K high-strength carbon, in the form of a Twill 2x2 type of weave and a weight of 200 g/m2. The composite was cured using a conventional prepreg technique involving a vacuum bag. The heating temperature was maintained at 80 °C for 360 minutes, with a heating and cooling rate of 1 °C/min. The vacuum pressure was set at 0.09 MPa throughout the whole process time. The stabilizer (9), mast (6), and camera mount (4) were made of three layers. The battery support bed (5) and the front engine arm module (3) were made of two layers. In addition, local reinforcements, (1), and (2) shown in Fig. 4, were used. Making the item from only three layers, a flat reinforcement was also added and inserted inside. Due to the need to run more electrical wires along the channel (7), it was deepened from 3 to 4.5 mm. A portion of the wall in the rear part of the fuselage (8) was also cut out with rounding. The biggest modification was made inside the fuselage by inserting a flat floor for the batteries in the second test object, which in the previous version had bends routed along the fuselage.

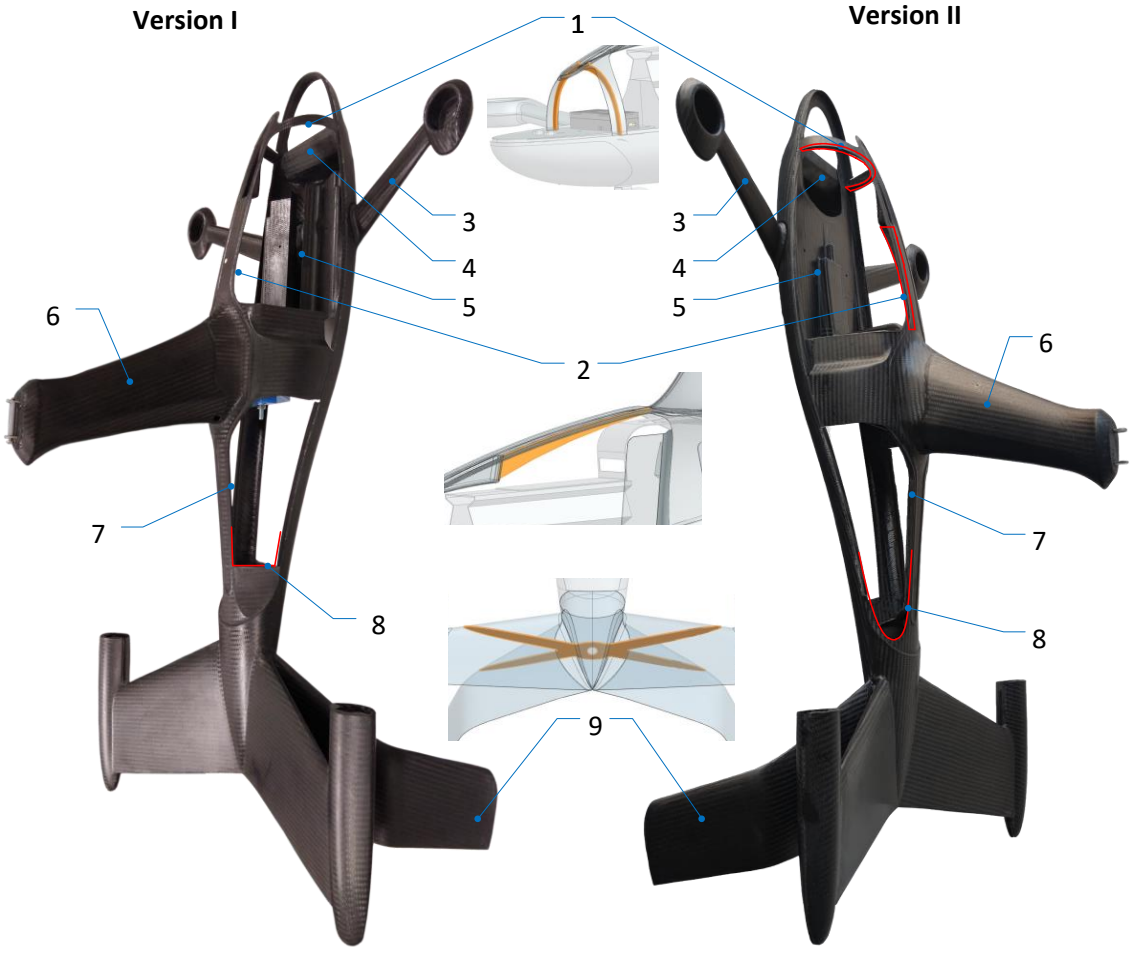

Fig. 4. View of the modifications made in Version II compared to Version I.

3. FORCE CONTROL SYSTEM CONCEPT, TEST BENCH AND DIC SYSTEM DESCRIPTION

The XGyro measurement system combines a strain gauge measurement and an ARAMIS digital image correlations system for studying the deformation of the various components of an unmanned aerial vehicle. It includes a control and load control subsystem for which a set of National Instruments equipment, with LabVIEW software, is responsible. The ARAMIS measuring subsystem is based on Digital Image Correlation and a parameterization subsystem. Fig. 5 reflects the whole process in a schematic way.

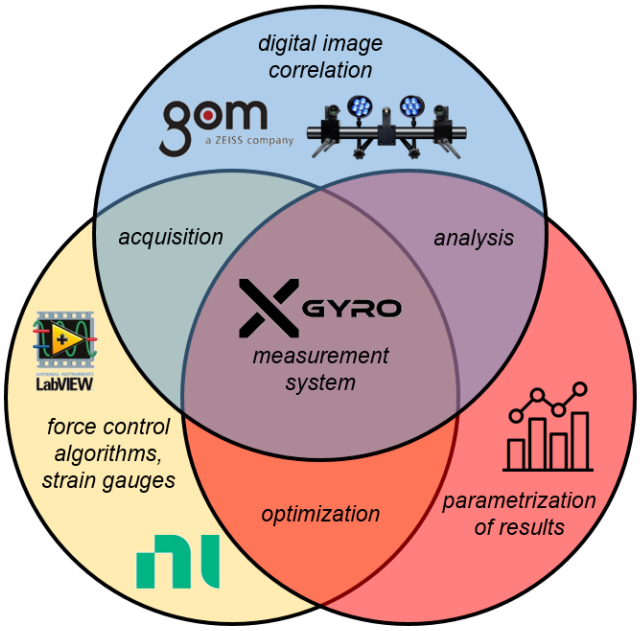

Fig. 5. General diagram of the XGyro measurement system.

The designed test bench should allow for the loading of the unmanned aircraft fuselage in accordance with the actual operation of the propulsion system. Therefore, it was necessary to predict the way of loading from the main rotor, tail rotors (in extreme positions, i.e. vertical and horizontal) and front rotors (only in vertical position). A diagram of the fuselage loads is shown in Fig. 6. The green arrows illustrate the direction of the loading force. In the case of vertical take-off, vertical flight or hovering, the vectors (S_1), (S_2), (S_3) and (S_4) work as shown in the figure, i.e. upwards. In the case of horizontal flight, the forces (S_5) (S_6) and (S_7) act as shown. The indicated force vectors are generated by separate servos. The tested fuselage is dedicated to the object, with a maximum take-off mass equal to 5 kg. Thus, it is assumed that when simulating horizontal flight, the rotor head should be pulled with a force corresponding to this mass to balance the gravitational force. On the other hand, during hovering, when the main rotor is unloaded, the arms on which the forces (S_1), (S_2), (S_3) and (S_4) are applied will be loaded with a force corresponding to a mass of 1.25 kg (each arm). These are values that can be multiplied depending on the flight condition. The flight dynamics and inertia that will occur during the flight affect the actual loads on the structure. Therefore, the stand was equipped with much more powerful servos, which generate a torque of up to 35.5 kg/cm for ($S_{1\text{-}4}$) and (S_7) and up to 25 kg/cm for (S_5) and (S_6). This means that at a radius of 1 cm, the first servo can lift a mass equal to 35.5 kg.

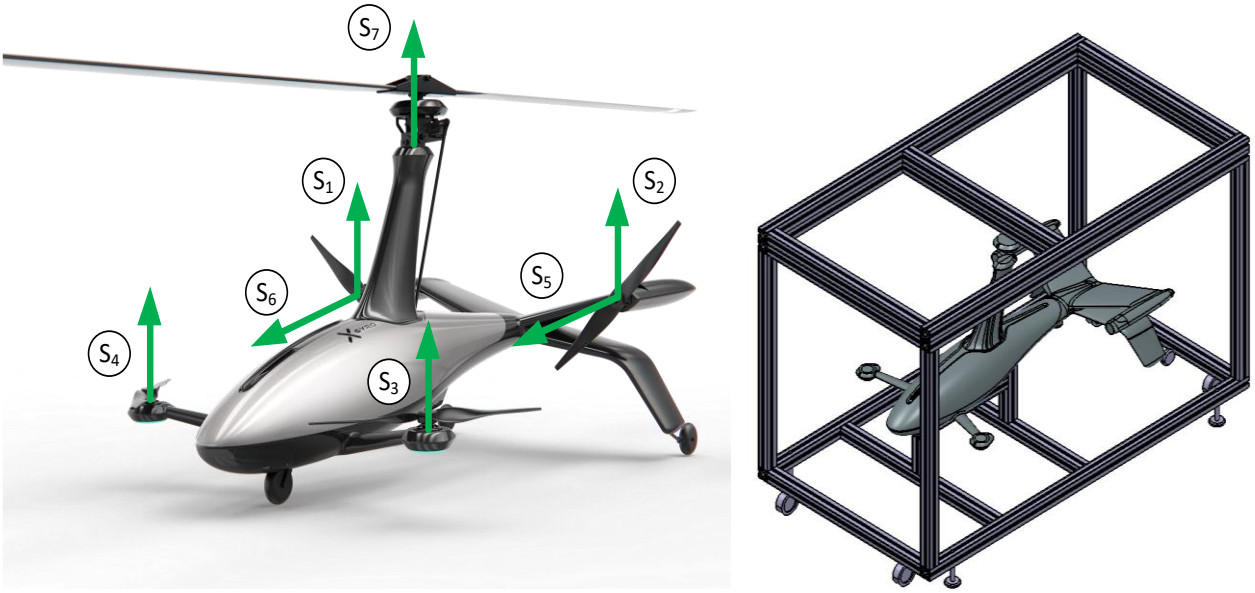

Fig. 6. The required load configuration for the designed test bench (on the left) and view of the modelled support structure for strength tests - isometric view (on the right).

The test object can be loaded with forces applied at seven different locations (Fig. 6). The loading system for one of the locations is shown in Fig. 7. The forces are generated using rotary servos (3). Servos generating a load of 35 kg/cm were used for forces acting in the vertical direction, while 25 kg/cm was used for forces acting horizontally. Circular orbits (4) were

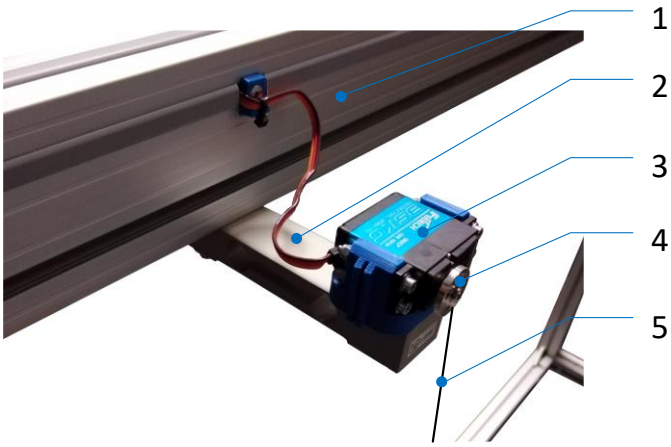

Fig. 7. The method of mounting servos on strain gauges.

attached to the rotary servos, onto which a rope (5) was coiled by rotation while producing a deformation of the test object.

To measure in real-time the force with which the system acts on the test object, the servos (3) were mounted on strain gauges (2) using specially designed and manufactured adapters. The forces generated are transmitted through the strain gauges, allowing them to be read and recorded. Strain gauges at the other end are mounted to the support frame of the test rig.

To develop a dedicated test rig for an unmanned aerial vehicle with the proposed configurations, a program was created in accordance with the block diagram shown in Fig. 8.

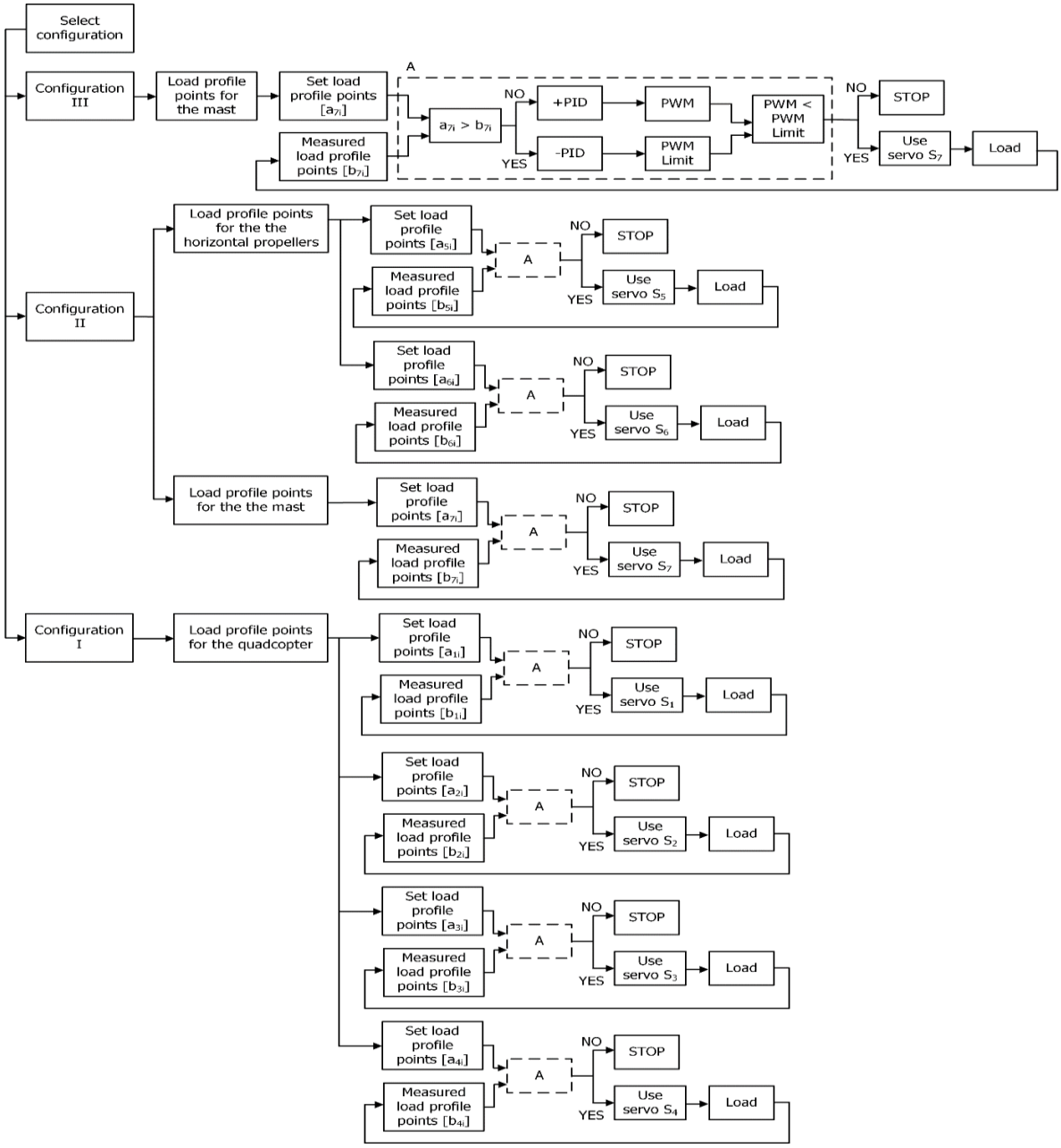

Fig. 8. Block diagram of the program created for setting loads on the unmanned aerial vehicle tested.

The test bench was built using National Instruments measurement devices and LabVIEW software. The instrumentation included NI-9237 measurement cards installed in a NI cDAQ-9171 chassis. The servos were controlled using an Arduino Nano module. They were attached to the frame by beam load cells. This solution provided control over the applied load. The control system of the test rig for simulating force loads acting on the XGyro research aircraft fuselage model was developed in the LabView environment, and a block diagram view of the program performed in it is shown in Fig. 9.

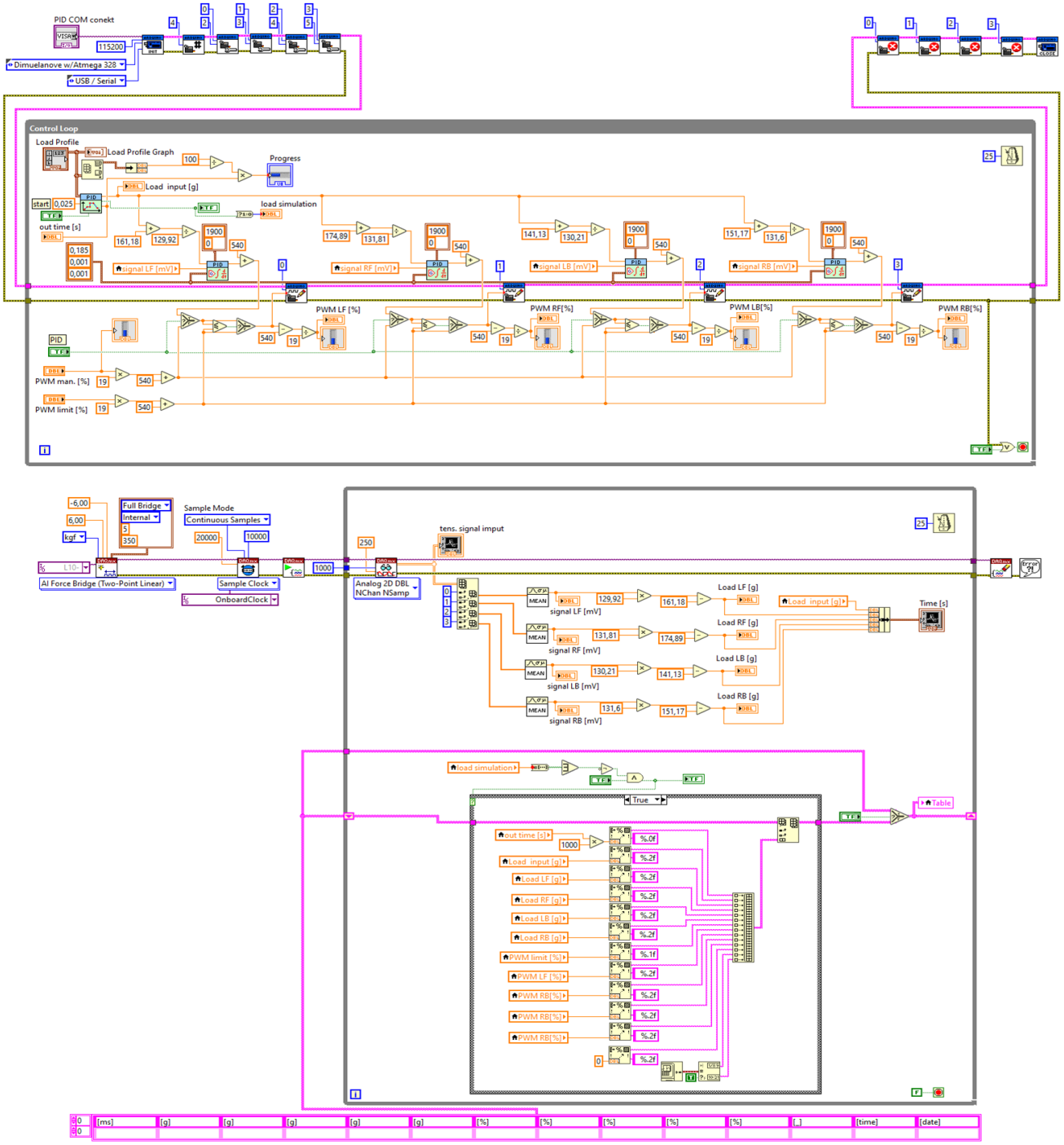

Fig. 9. Block diagram view in LabVIEW.

Fig. 10 shows the front panel of the program developed. Three key parts can be distinguished in it that interact with each other. The first is formed by the system for forming the load profile, applied at the nodes. It consists of a table and a load profile graph. The first column of the table contains the time expressed in seconds, and the second column contains the value of the applied load expressed in [N]. This makes it possible to create arbitrary load profiles for the aircraft fuselage, reflecting single flight states or scenarios consisting of several stages.

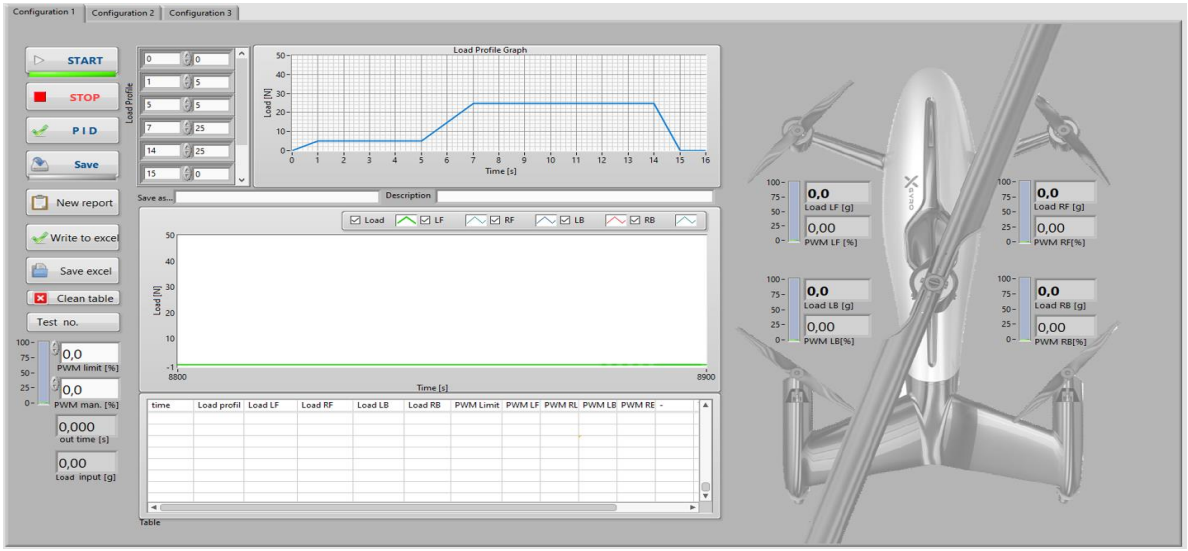

Fig. 10. Front panel view for active configuration I.

The prepared load plan as a function of time is visualized in the "Load Profile Graph". The tests of the structure conducted using ARAMIS simulated a scenario consisting of four phases: preparation, takeoff, flight and landing. Another part of the program is a measurement and execution system correlated with seven force generation systems. Each of them consists of a servo, a force sensor and a rope connecting the servo to the aircraft fuselage. The program takes a force measurement for a given node and then compares it with the force profile setpoint. Using the PID, the algorithm controls the PWM value of the servo motor. Feedback control enables precise, repeatable load setting at nodes. It also protects against overloading the hull structure. The PWM values acting on the motor and the load values applied to a node are shown by the indicators on the right side of the control panel.

The last part of the program is a system for recording data and creating reports on the tests carried out. Load values and PWM values of individual servos are recorded and saved. The registration takes place automatically after activating the "Save" button with a fixed time step of 25 ms. The obtained results are saved in a table visible on the front panel of the program. The characteristics of the loads in time are adjusted on a graph located in the central part of the front panel. Each of the recorded files were exported to Microsoft Excel in the form of a report.

The measurement system thus completed, which includes the control and load monitoring subsystem; the ARAMIS measuring subsystem based on Digital Image Correlation, and the parametrization subsystem for the results obtained, can be seen in Fig. 11 and Fig. 12. The photographs show the fuselage during tests on the developed test bench.

Fig. 11. View of the test bench during tests – general view.

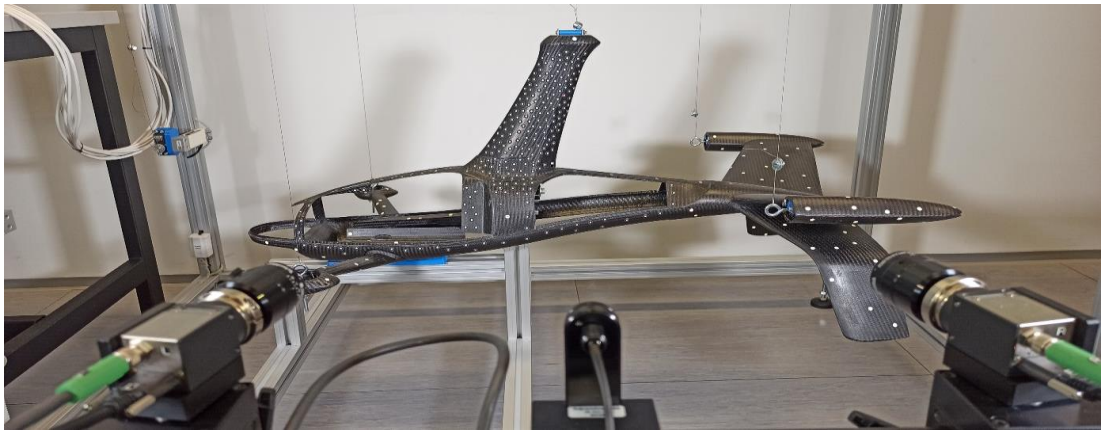

Fig. 12. View of the test bench during tests – view of the research object.

Digital image correlation (DIC) is a non-contact measurement method, based on the application of one (two-dimensional) or multiple (three-dimensional) cameras registering the studied object put in the measuring volume $x = [x,y]$ during the load generation phase. Monochromatic images and randomized speckle patterns or high-contrast reference markers (herein) allow the observation of the changes in the intensity of light reflected from the analysed object with a certain noise μ. The recorded frames (g(x)) are compared with the initial frame (f(x)) of the unloaded object to determine the residual (ρ(x)) (Eq. 1), which is the criterion of the images' compatibility related with their grayscale. The residual is needed to be as close to the noise as possible, which is accomplished by the differentiation of the residual and standard deviation of noise if Gaussian distribution is assumed. The result of such a comparison is the measurement of displacement field u (Eq. 2) [24], [3].

$$\rho(x) = g\big(x + u(x)\big) - f(x) \tag{1}$$

$$f(x) = g\big(x + u(x)\big) + \mu(x) \tag{2}$$

To ensure the appropriate operation of the DIC system, a set of preliminary activities must be accomplished. Later, the work of the DIC has to be synchronized with the test object and the eventual test bench, when it is needed to implement (like in this case). These operations ought to result in reliable and accurate data acquisition. Finally, data analysis has to be conducted on the collected data to determine the construction behaviour and assess if and how advanced changes are needed. The overall workflow during the implementation of DIC is presented in Fig. 13.

The preparation stage requires determining the initial work parameters of DIC system elements. Each of the two cameras is set up using different transformation vectors ($T$and T'), a different set of intrinsic and extrinsic parameters ($K$and K' matrices) and different coordinate systems. The alignment of cameras is connected with the third vector – the stereoscopic transformation vector (T_s), which merges (Eq. 3) the transformation vectors of the cameras used to fit the point observed by them simultaneously in the global coordinate system [6].

$$T_s = T'T^{-1} \tag{3}$$

To facilitate such transformation, epipolar geometry 19 has to be constructed between the cameras and the observed object. The cameras' fields of view have to intersect each other, and be located in a way that the plane can be constructed from the observed point and optical centres of cameras. This creates the epipolar lines on the virtual plane created by the images from cameras and in the area adjacent to the lines; the position of the point can be estimated.

The intrinsic and extrinsic parameters matrix consists of the properties of the cameras used and the image acquired by them i.e. the focal length, pixel size, distortion coefficients, cameras convergence angle and position [3]. On the basis of $K$and K', the position of certain 2D points m and m' combined in 3D, point M, is determined (Eq. 4 and 5) [6]. Moreover, the matrix components are decisive for the final dimensions of measuring the volume of the system and its image-resolving power.

$$\tilde{m} = KT\tilde{M} \tag{4}$$

$$\tilde{m}' = K'T'\tilde{M} = K'T_sT\tilde{M} \tag{5}$$

Thus, the $K$and K' matrices have to be established for the used visual system to enable the quantitative description of motion by DIC.

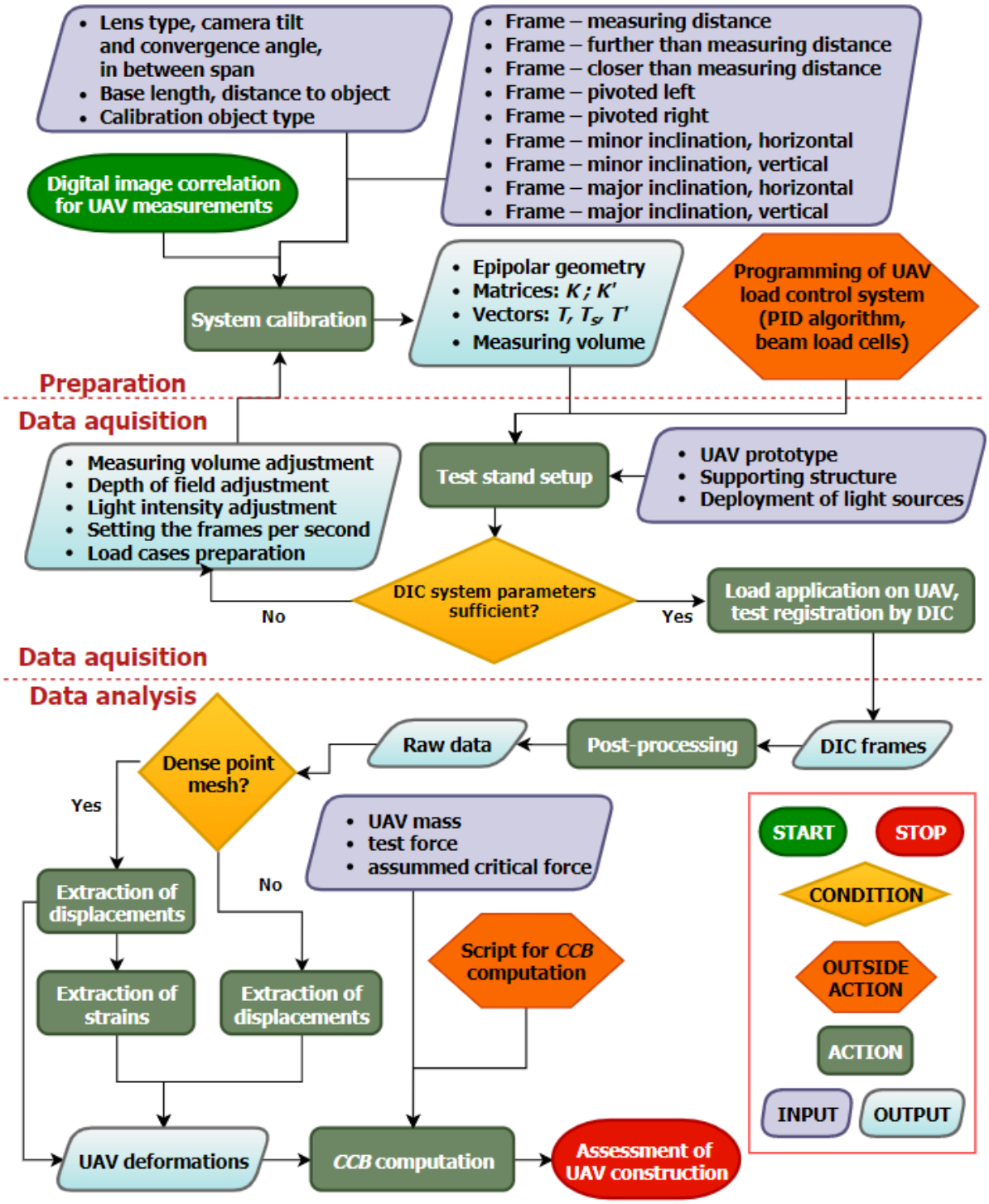

Fig. 13. Block diagram of operations done during DIC analysis of UAV in-work conditions response.

These are obtained using system calibration, which consists of cameras set up at a proper distance between each other and in the approximate distance from the object, where the epipolar geometry can be built. Also, the adjustment of image sharpness and the lens aperture is then conducted. Finally, the capturing of several frames at different distances and different angles in relation to the calibration object is performed. This gives the specific values of the parameters building the K and K' matrices, which allows the obtaining of the sub-pixel accuracy (typically $10^{-2} \div 10^{-4}$ mm [19]).

Based on the values obtained from calibration, the measuring volume and depth of field are determined. As these parameters cannot be changed without the conduction of another calibration, the object should be fitted to them. For the object, which has little possibility to scale down, the repeat of calibration to obtain more suitable parameters is unavoidable.

Finally, if the capturing of the whole object image is not possible, the observation of the object can be divided into zones. Also, the intensity of incident light has to be adjusted to facilitate the comparison of the greyscales and thus – the determination of displacements [8]. Dependent on the measuring volume, the size of reference markers has to be accordant as well. When the above-mentioned factors are checked, the experimental tests and data acquisition can commence.

For the reference markers dispatched on the investigated surfaces of the UAV, the raw data featuring (mainly) displacements and rotation angles were collected and further analysed. For the cases where a large number of points allowed the creation of a dense mesh to serve as the base for surface components, the additional data was collected by the use of the stock functions of post-processing software (GOM Correlate v.2020 Hotfix 6). However, for the collection of data, being the more complex form of raw measurements, the creation of a proprietary script is needed. Thus one was formulated for the coefficient of construction balance (CCB), described later in the text. CCB was introduced by the authors for a quantitative presentation of the construction modification effects. The implementation of the script based on the equations submitted above allowed us to obtain automatically the assumed assessment criterion at the moment of data post-processing and enabled the prompt comparison of two construction variants.

The DIC system was built using two 12 MPx cameras equipped with S50 lenses (focal length of 50 mm, made by Schneider-Kreuzbach, Germany). The cameras were fixed on an adjustable bar (800 mm in length, provided by GOM, Germany). Calibration was conducted on a CP40-200 plate (GOM, Germany). DIC was calibrated in two configurations to address the issues with acquiring the points located beyond the depth of field during the prior analyses:

- Configuration no 1: camera resolution: 4096x3000 pix, measuring volume: 255x185x185 [mm], camera convergence angle: 25°, calibration deviation: 0.078 pix (max. allowable: 0.100 pix) resulting in measurement uncertainty of 0.005 mm;
- Configuration no 2: camera resolution: 4096x3000 pix, measuring volume: 350x260x260 [mm], camera convergence angle: 25°, calibration deviation: 0.034 pix (max. allowable: 0.100 pix) resulting in measurement uncertainty of 0.003 mm.

To carry out the most detailed analysis of displacements of the object as a result of particular load scenarios, it was decided to analyse selected fragments of the structure, subjected to the highest loads and potentially the highest risk of damage. In the case of vertical loading of the mast, displacements and their base connected adhesively with the fuselage was observed (Zone I in Fig. 14). In the remaining variants of vertically directed loads, displacements of the front part of the fuselage together with structural elements in the area of the equipment chamber (Zone II in Fig. 14) and the area of the fuselage tail-plane connector (tail section) (Zone IV in Fig. 14) were analyzed. Additionally, displacement analysis was performed for the front arms and the arm deflection was evaluated as a result of the bending moment occurring during vertically directed loading (Zone III).

Fig. 14. Zones of the test object observed during strength testing.

The created test stand is multi-component. It consists of a load-setting system (a system of servos connected to strain gauges) and a DIC system, i.e. two image-recording cameras and an image-processing system. Each of the subsystems has is its own accuracy. The accuracy of material deformation measurements were made using the Aramis system and depended on several factors: image resolution, sizes of the correlation window, conditions of specimen surfaces and lighting conditions. The image-recording-and-processing system applied has a measurement uncertainty of no more than 0.005 mm. Compared with the recorded deformation range of 1-4 mm, displacement accuracy was considered to have no effect on the defined parameters of mechanical behavior of both UAV models. The tests were carried out in a laboratory where the contribution of light sources of highly variable intensity, e.g. sunlight was kept to a minimum to conduct repeatable tests and reduce any factors that could affect the reliable reading of the measurements. What is more, several light sources of similar intensity were used. They were in several locations to remove shadows on the object that could potentially change the gray scale perceived by the lenses of the DIC system. The external forces applied were measured with beam strain gauges with a measuring range of up to 6 kg (arm load) and 10 kg (mast load) in class C3. The devices showed a combined error of $\leq \pm$ 0.023 % so the load is set to an accuracy of 1.38 g and 2.3 g at full measurement range, which means the force applied to be 0.0135 N and 0.0226 N, respectively. The above accuracies were considered sufficient for the case.

4. RESULTS AND DISCUSSION

A progressive deformation analysis was conducted separately for the defined zones of the UAV. From the reference markers placed on the studied surfaces, the magnitudes of displacements were acquired, post-processed and analysed. An investigation of each recorded zone was conducted to acquire a description of changes in structural behaviour under various loads. The same measurements were conducted for the new version of the UAV to compare the effect of changes in the construction.

4.1. Relation of measured displacements to the load used for the first version of the UAV

The coupling of displacement measurements and input data of the force control system by the time markers registered in both subsystems allowed the authors to investigate thoroughly the response of UAVs under specified load cases. Based on the measurements collected, one can state, that the increase of the load produced by servomechanisms (simulating the operation of rotors) provides a further growth of the observed deformations in the inspected zones of the UAV (Fig. 15). The above-mentioned statement is true for all considered cases. Considering the fact that the assumed take-off mass for the analysed construction is 5 kg (49 N of force equivalent), in all of the cases the UAV preserved its stability and showed no signs of near-failure or a failure state. This means the construction can be dedicated to work in more demanding conditions or it can be further optimized to reduce its mass.

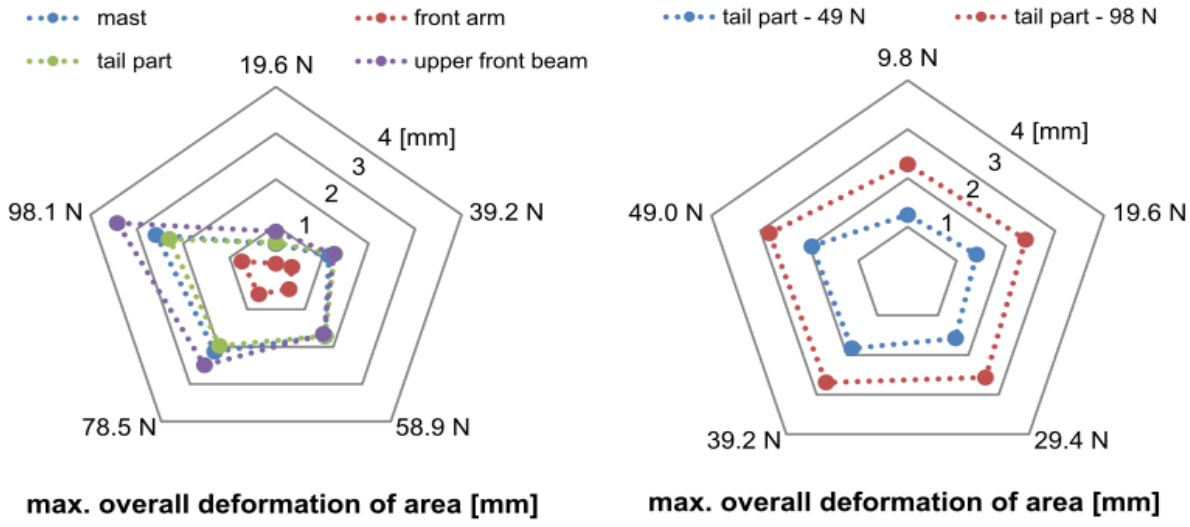

Fig. 15. The overview of UAV deformations in the dependence of used force – at the moment of take-off and vertical flight (on the left) and the behaviour of the tail section during horizontal flight (on the right).

The description of deformations distribution during the progressive deformation analysis was presented for the highest loads only due to a lack of differences in the behaviour between each of the force magnitudes used – a distribution of displacement vector components in the zones studied for all load magnitudes was similar. Additionally, the share of each vector component was underlined to prepare a more accurate analysis of the UAV's response.

4.2. Description of the first version of UAV fuselage response during take-off and movement

The deformation analysis, using reference markers, allowed the collection of exact displacement values for the places of their attachment. Nevertheless, for zones where markers are densely placed, there is a possibility to extrapolate a surface map and analyse the magnitudes. To do this, the determination of the close proximity of two certain points and their mutual locations is needed.

Considering the displacements captured on reference markers at the mast region (Zone I in Fig. 14), the main effort is placed on moving the mast horizontally. The material response in the vertical direction is the secondary source of the deformation magnitudes displayed. In comparison to the above-mentioned components, the lateral deflections present minor values (up to 0.3 mm) and they are distributed uniformly on the studied surfaces of the UAV. However, the composite structures are sensitive to out-of-plane loads, so this component should be cautiously monitored – regardless of the stability issues that are expected. The overall movement of the mast was equal to 2.589 mm at the peak point.

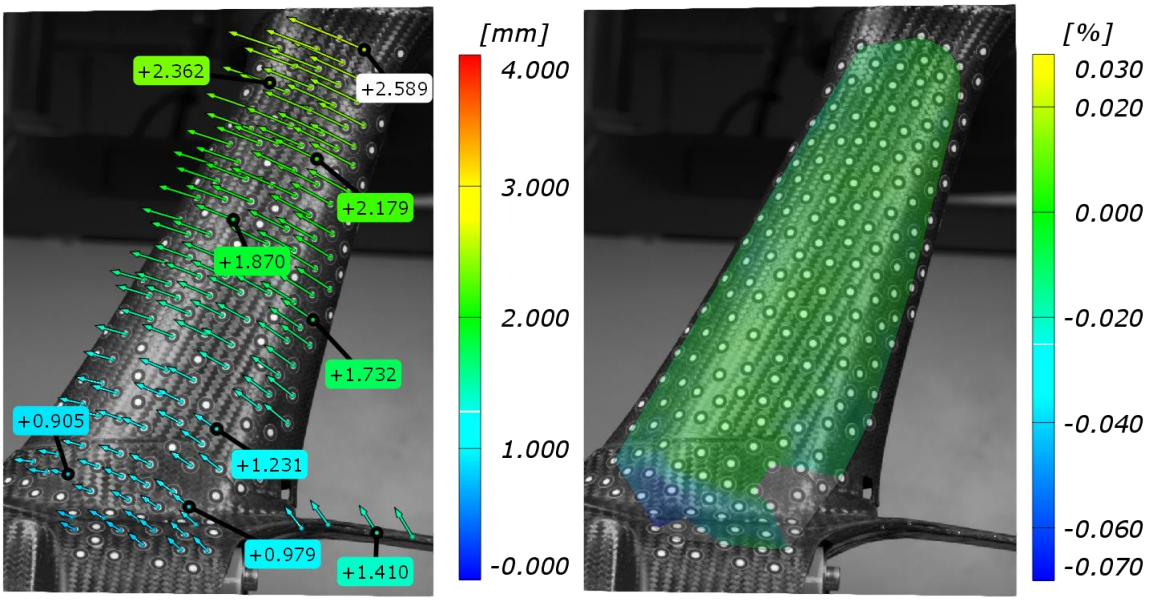

Fig. 16. The displacement vectors (left) and major strain (right) correlated with the image of the original mast at the highest load.

The occurrence of deformations towards the top of the mast was observed, mainly due to the induction of bending by an acting force placed at the most distant point from the UAV fix zone. The relatively uniform distribution of displacements in the zone of mast-to-fuselage joint confirms the good quality of adhesion between the structures of UAVs. Nevertheless, a strain analysis 20, 10 of the link between the mast and upper tail beam was made on the virtual surface created from the mesh of scanned points, which were later transformed in the strain map (Fig. 16). The strain distribution suggests that the above-mentioned connection link is the point most prone to fracture.

The significant distance between the floor of the fuselage and its upper front beam meant that DIC was unable to observe both areas simultaneously due to the limited depth of field 13 of the cameras used (Zone II in Fig. 14) in calibration configuration no 1 (Section 3). However, the measurement for the largest magnitude of force, being mass equivalent, was performed to identify the behaviour of the upper front beam (Fig. 17). The highest detected deformations in the whole UAV were reported there – as much as 6.35 mm in the most critical place. Due to these results, the enlargement of the stiffener below the beam and the increase of the cross-section is highly recommended.

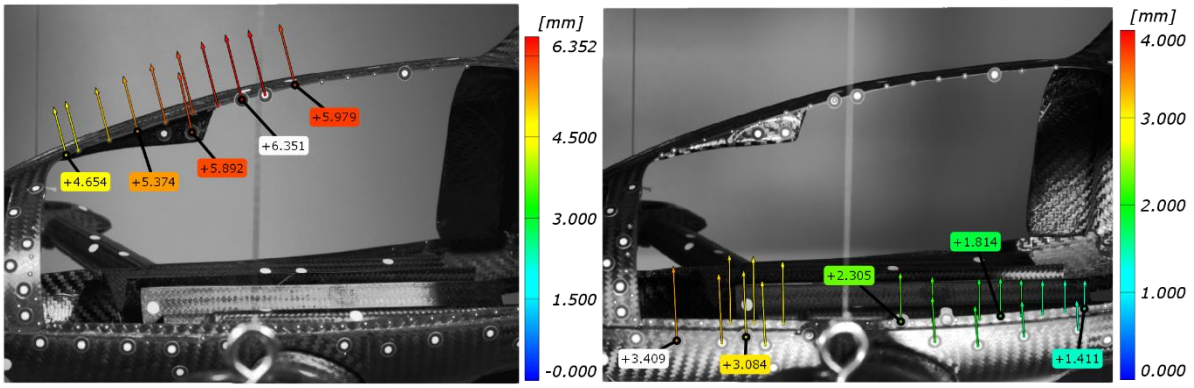

Fig. 17. The displacement vectors correlated with the image of the front part of the original (first version) fuselage for the highest value of the force – vertical flight.

The walls connected to the floor and battery sockets tend to deflect outside the original contour of the fuselage, however – like in the case of the mast, the lateral displacement magnitudes are marginal (approximately 0.4 mm). Similarly, the horizontal component of overall deflection is a minor factor (maximum 0.5 mm) influencing the overall response of this segment of UAV. The main effort is made in the vertical direction, where along with the growth of the distance from the fixed point, the displacement increases. The above-mentioned description is in accordance with Fig. 17, where it is visible that the displacement vector is mainly oriented vertically – the maximum displacement of the analysed zone is equal to 3.409 mm.

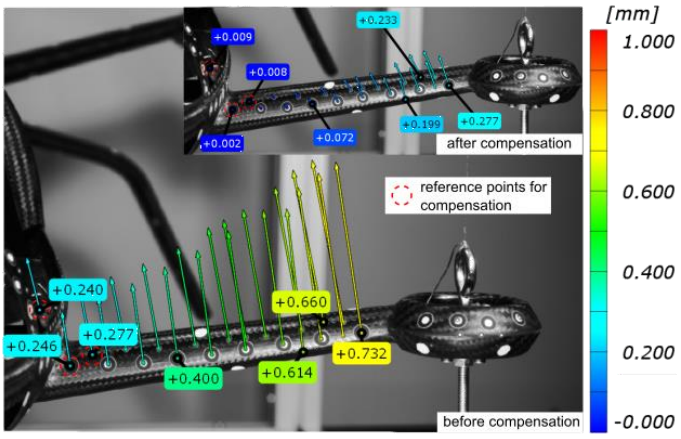

Fig. 18. The displacement vectors correlated with the image of the front arms (first version) - vertical flight.

Upon considering the front arms' behaviour (Zone III in Fig. 14), the movement of the whole construction and the movement of the arms themselves can be analysed. To consider the second factor, the compensation of measurements is needed. The selection of points located near the fuselage allowed for the establishment of a new reference point in the data acquisition and the checking of the actual deflection of the beam joining the nacelle with the fuselage. Fig. 18 presents, how significant can be the difference while considering the same element with and without the compensation. Recognition of deformations in the separated area may affect the assessment if any of the considered areas need constructional changes and which one needs them.

The largest displacements are visible away from the fuselage (raw data – 0.732 mm, after compensation – 0.277 mm). Upon considering which component of the investigated vectors is the most significant, the highest displacement in principle directions was observed for the vertical axis. During take-off, the arms tend to be dragged backwards (max. 0.1 mm). Also, the horizontal component of the analysed vectors is marginal (approximately 0.1 mm).

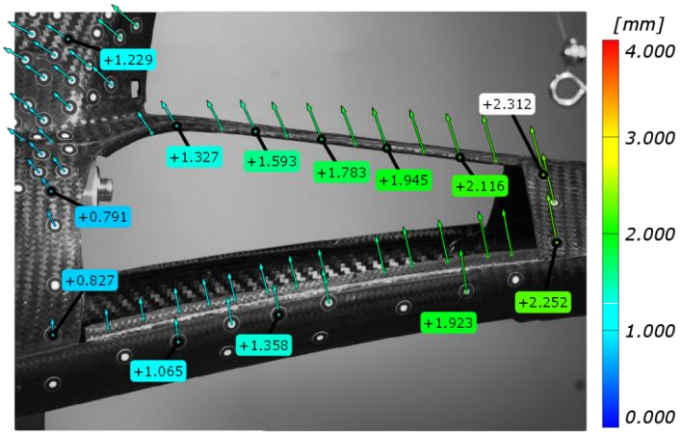

Fig. 19. The displacement vectors correlated with the image of the tail section of the original UAV - vertical flight.

The observation of the tail section of the UAV (Zone IV in Fig. 14) resulted in the registration of 2.312 mm of peak overall

deflection of this segment (Fig. 19). The main difference is visible in the vertical direction – again, the farther away from the fixed point, the greater the deflection. Also, a significant share of the horizontal component was observed. The movement forward was rising against the increasing distance from the fixed point. The points set on the upper tail section tended to displace horizontally further than those marked below.

To compare the UAV response during take-off and movement, the deformation of Zone IV (Fig. 14) was recorded again. The map of displacements measured while the UAV was loaded is presented in Fig. 20.

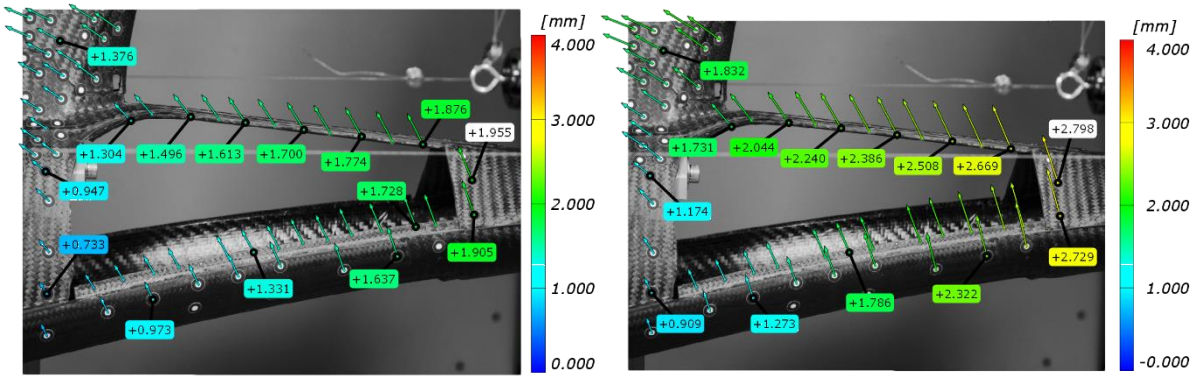

Fig. 20. The comparison of the original UAV tail section during the movement simulation under 49 N (left) and 98 N (right) of load acting on the mast – horizontal flight.

The action of motors enforcing the forward movement of the UAV changed the tail deflection by 21% (for 98 N on the mast) compared to the vertical movement only. The changes in the vector components are minor, contrary to the measurements presented in Fig. 20. The vertical component is still the largest, however, the share of the horizontal vector component increased significantly, from 1.078 mm to 1.749 mm for the highest load case.

4.3. Presentation of changes introduced to UAV construction

Based on the prepared DIC measurement, a set of changes in the UAV's construction was introduced. Also, to address the issues met while analyzing a front part of the fuselage, the DIC was recalibrated to the state (calibration no 2), where a greater depth of field was able to be reached. Upon comparing the data acquired during the next measurement series (Fig. 21) with the readings from the earlier version of the vehicle, a significant decrease in the displacements was observed for the elements which had been selected to be strengthened. In the case of the front arms, which were subjected to weight reduction, the increase in deflection is visible. However, the authors claim this value is sufficient for the safe operation of the aircraft.

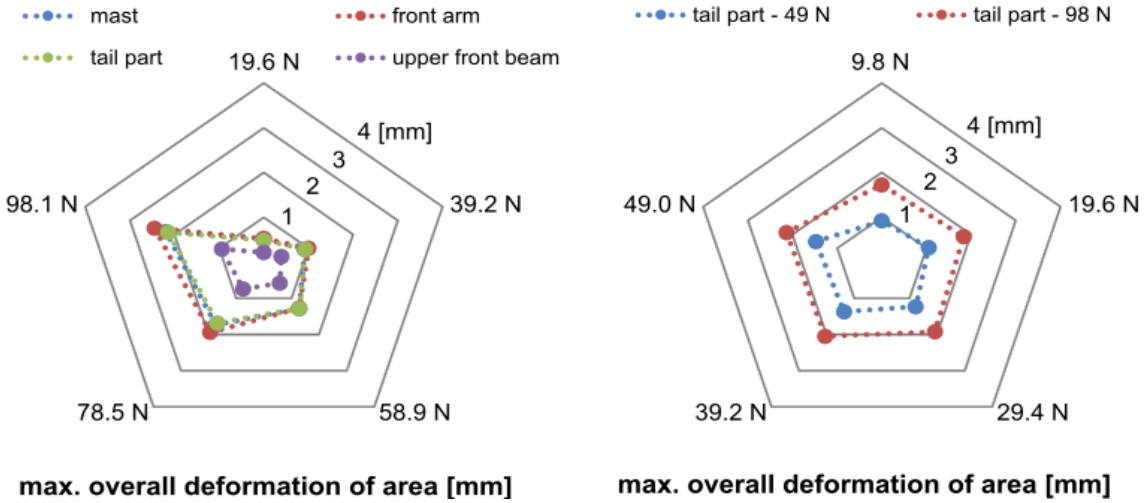

Fig. 21. The overview of UAV deformations in the dependence of used force at the moment of take-off (left) and the behaviour of the tail section during the flight (right).

As in the previous part of the research, a detailed analysis of construction movement was performed to identify the main factors acting on the construction. Apart from the vector components description, a comparison to the characteristic points of earlier versions of the UAV was done.

The mast was weakened by removing one layer of CFRP fabric. The results of modification are presented in Fig. 22. The peak deflection determined from reference markers is significantly lower than the one for the original structure (15% decrease). The distribution of the vector components did not change significantly – the share of vertical and horizontal parts was similar to the original construction, however, the lateral component was reduced by 33%, to approximately 0.2 mm.

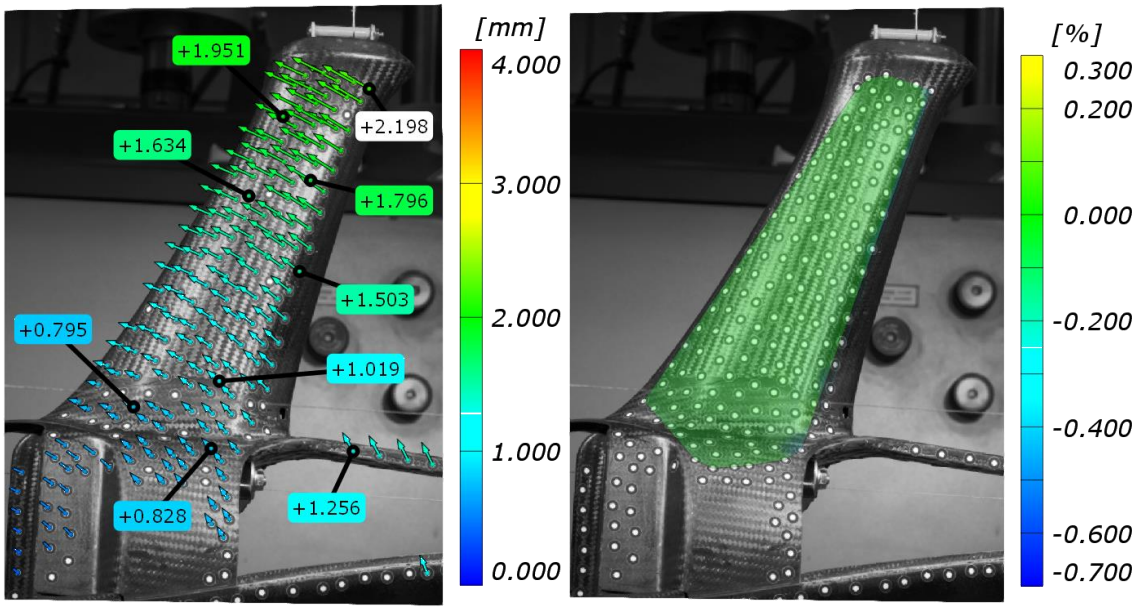

Fig. 22. The displacement vectors (left) and major strain (right) correlated with the image of the modified mast at the highest load.

Also, the changes are visible while considering the strain analysis – the values of major strain are marginal, contrary to the earlier version of the UAV. Moreover – the strains were significantly reduced in the area of the mast-fuselage joint. There are two reasons for such a state – the first can be the presence of an additional CFRP layer, and the second may be better adhesion between two elements of the UAV fuselage.

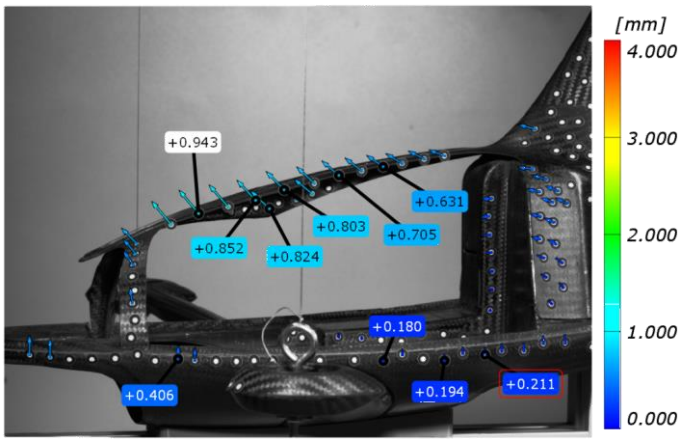

Fig. 23. The displacement vectors correlated with the image of the front part of the optimized fuselage for the highest value of the force.

Due to the high deflections of the upper front beam, and the deck overall, an upper bar stiffener was added to optimize the response of this part. The greater span of DIC cameras allowed the observing of the item with a greater depth of field, so the simultaneous registration of upper bar movement and the deck from the front part of the fuselage was possible (Fig. 23), which facilitated the further analysis significantly and allowed the recording of a similar amount of data on a lower number of frames (lesser size of raw file).

The peak deflection of the front part of the deck was reduced 8.5 times – from 3.4 mm to 0.4 mm. Almost the same level of displacement reduction was spotted for the upper bar – from 6.35 mm to 0.85 mm, at the same measurement point. The peak deflection was shifted forward, to the point where the stiffener height is the lowest. Also, the distribution of vector components was changed – the share of horizontal and vertical movement was equalized. The share of lateral deflections was reduced by 60%, from 0.4 to 0.16 mm.

Due to the relatively low deflection of the front arms, the decision was made to lighten this structure by the subtraction of

two CFRP fabric layers. The measurements after modification (both – original data and data after compensation made on the beam's fixture area) are presented in Fig. 24.

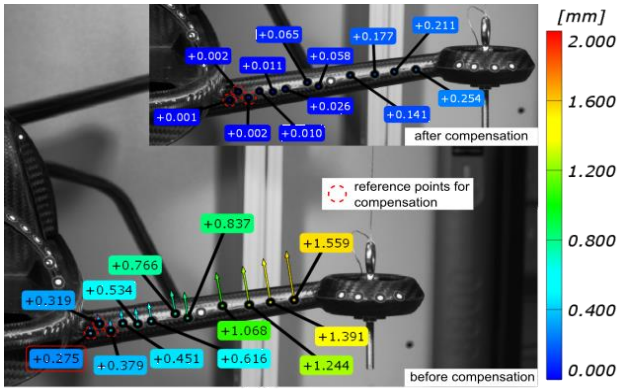

Fig. 24. The displacement vectors correlated with the image of the motor nacelles.

The overall deflection of the UAV in the monitored position doubled in comparison to the earlier version. After preparing the compensation for the beam fixture, the deflection remained at a similar level to earlier. This observation presents two possibilities. Firstly, the main strain of the material is located at the central part of the beam, which is linked to the fuselage. Secondly, the uncompensated measurements presented the movement of the whole construction.

In the case of tail section modification, the upper beam was strengthened and its shape was modified due to the greater exposure of the load compartment in the zone next to the fuselage-tail nacelles connection. Also, the tail nacelles were weight-reduced. Fig. 25 presents the overall movement analysis of the modified element of the UAV.

The reinforcement of the tail beam resulted in a 7.5% of displacement reduction in the peak location. What is worth mentioning, the analysed peak point is projected further from the fixing zone than the one analysed for the first version of the UAV. Comparing the peak point from the original construction with the point placed close to the above-mentioned one (2.028 mm of deflection), the reduction reached up to 12%. The distribution of vector components, in comparison to the earlier version of the aircraft, did not change significantly – the advantage of vertical displacement, supplemented by a significant shift toward the fixed point and an insignificant share of lateral deformations.

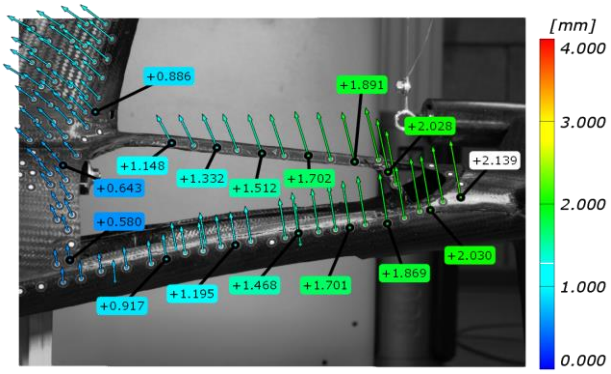

Fig. 25. The displacement vectors correlated with the image of the tail section of the original UAV.

Again, the comparison of the UAV tail section working in conditions of horizontal flight was done for two variants of mast load. Fig. 26 shows that the deflections were significantly limited in comparison to the former construction. The peak displacement is limited by 24% for both load cases. Considering the point close to the peak point of the earlier version, the reduction is equal to up to 30%. Also, a slight change in vector components distribution was observed – the horizontal and vertical displacements show lower differences than before. As for the earlier version, the horizontal component almost doubles its magnitude (0.845 mm to 1.536 mm for 98 N on the mast). However, the vertical component is the largest compared to the other components of the vector.

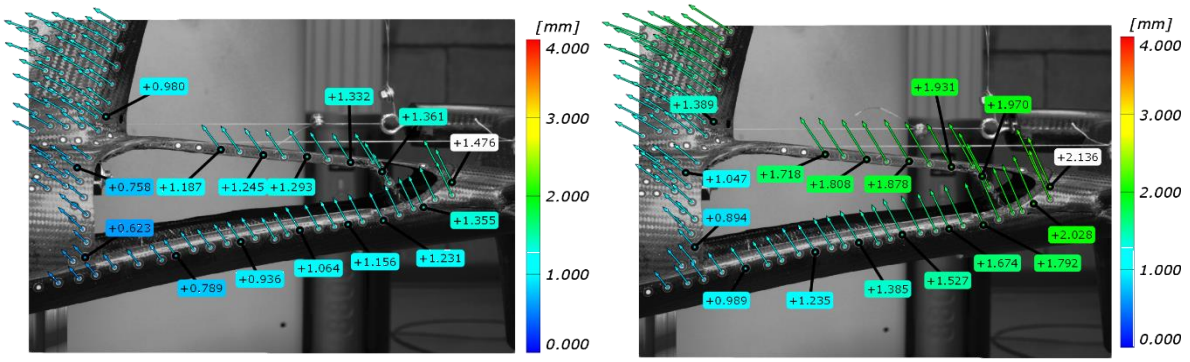

Fig. 26. The comparison of the modified construction of the UAV tail section during the movement simulation under 49 N (left) and 98 N (right) of load acting on the mast – horizontal flight.

4.4. The assessment of revision efficiency

The optimization of UAV construction was performed based on two conditions: 1) the reduction of peak deformations and average deformation within a zone (A_K variable, Eq. 6), 2) the reduction of overall vehicle mass (m_{UAV}). To present the objective measure of change efficiency, which contains the above-mentioned criteria, the construction response equivalent (*CRE*) was introduced (Eq. 7). The proposed assessment criterion includes the deformation data analyzed earlier, test conditions meant as applied force (F_{test} = 19.6 N; 39.2 N; 58.9 N; 78.5 N; 98.1 N for take-off and F_{test} = 9.8 N; 19.6 N; 29.4 N; 39.2 N; 49 N for horizontal movement) and work conditions assumed for this construction at the conceptual stage as the expected starting mass of the UAV, which was translated to force magnitude (F_{start} = 49 N). Based on *CRE*, the coefficient of the construction balance (*CCB*) was defined (Eq. 8) to include the changes in UAV mass. The CCB is desired to be as high as possible, provided that $m_{UAV} \rightarrow min$ and $CRE \rightarrow max$.

$$A_K = \left(\frac{\left(\frac{\sum d_i}{i-1} - \frac{d_{max}}{i-1} \right) * 1}{d_{max}} \right) \tag{6}$$

$$CRE = \frac{\left(\sum \left(\frac{A_K * F_{test}}{F_{start}} \right) \right) * 1}{K} \tag{7}$$

$$CCB = \frac{CRE * 1}{m_{UAV}} \tag{8}$$

where:

A_K – deformation variable [unitless]

CCB – coefficient of construction balance [1/kg]

CRE – construction response equivalent [unitless]

d_i – magnitude of reference point deformation [mm]

d_{max} – maximum deformation for the load case [mm]

F_{start} – force equivalent of starting mass [N]

F_{test} – force equivalent of tested mass [N]

i – number of reference points

K – number of load cases

m_{UAV} – overall mass of the UAV [kg]

Figure 27 presents the results of script computations for CCB and the correlation of CCB to the work conditions for both UAV variants. The CCBs from the experiments were compared to the CCB calculated based on the following assumptions, which were made at the beginning of the XGyro project: 1) The construction should resist the force equivalent of a take-off mass equal to 5 kg (conceptual F_{test} = 49 N), 2) The construction cannot be heavier than 1.2 kg (conceptual m_{UAV}). The deformation variable for this specified case was assumed as the mean value from all measurements gathered. Also, the CCBs for each load case were calculated to show which modification was the most crucial for optimizing the structure.

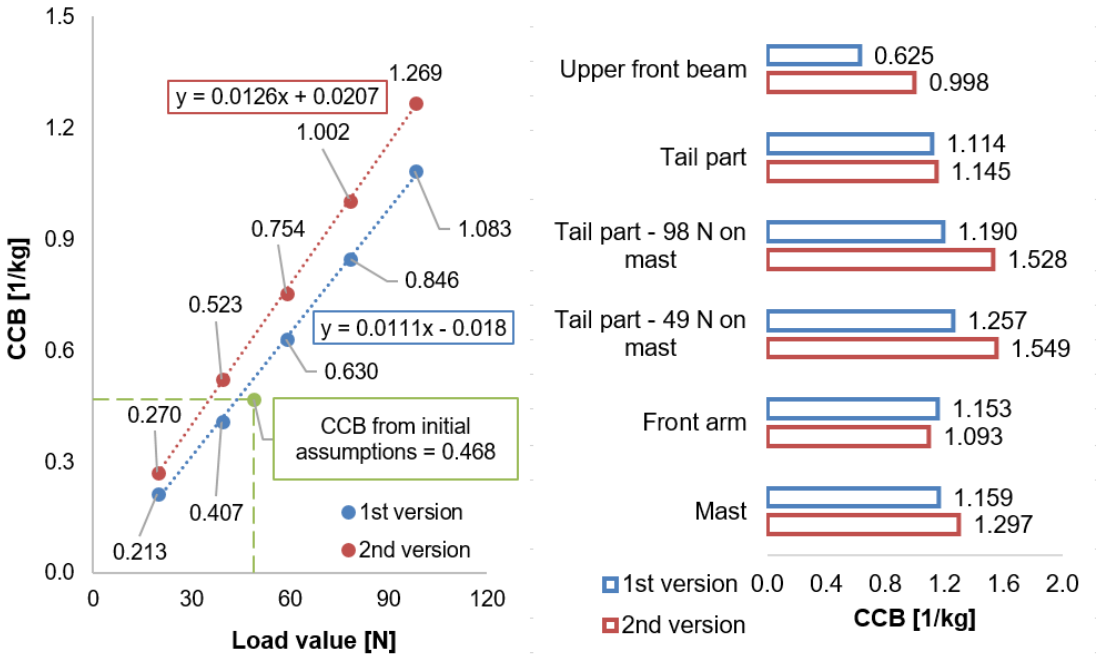

Fig. 27. The relation of CCE and applied force (left) and the efficiency of construction changes divided into investigated zones for 98 N of force (right).

The charts show clearly, that for all of the load cases, the CCB of the modified construction is greater and grows at a higher rate than the CCB of the first version. Upon analysing the changes in CCBs for each studied zone, a significant improvement was observed for the majority of investigated cases. The most important change was the stiffening of the upper beam in the front part of the UAV – this operation ensured a 60% increase in the construction balance coefficient. Despite the additional material increasing the vehicle's mass, the limitation of deflection was major.

The comparable results were obtained for the tail section loaded as if for the UAV's take-off. However, a slight decrease in the CCB was observed for the front arms. This was connected with the large mass reduction in this part (the use of two plies of CFRP instead of four), which caused the increase of deformations in this area. Based on acquired data and the adopted assessment method of construction optimization, the authors claim that the optimization of the UAV construction has been conducted successfully, not only in terms of deformation reduction, but also mass reduction – from m_{UAV} = 1.065 kg to m_{UAV} = 0.858 kg.

5. SUMMARY AND CONCLUSIONS

This work presents the authors' method that allows the analysis of the deformation of a fuselage manufactured from CFRP for the construction of an unmanned aircraft characterized by increased functionality resulting from the combination of the advantages of a gyrocopter and a multicopter. The system required an extensive test plan corresponding to the loading conditions arising during specific phases of flight. For the analysis, a DIC system was used, as well as a test rig designed and built by the authors, equipped with a dedicated control system. Based on the results presented, the following statements can be made:

- The developed PID control algorithm and the stand made by the authors are capable of effectively simulating the operating conditions that result from the operation of the engines with the propellers provided in the design.
- The use of the DIC system made it possible to determine the displacements and deformations at specific points on the first version of the structure. Based on these readings, a description of the UAV fuselage's response to given loads was created, modifications were made and a second prototype model was produced.
- Displacement analysis performed on the second model showed that the modifications resulted in lower deflections in the composite structure under consideration.
- To objectively determine the quality of the modifications to the structure, the authors proposed a CCB factor. The CCB parameters calculated for the first and second versions of the structure indicate that both structures meet the initial assumptions of the XGyro design. In addition, the second version of the design shows an average of 22% more effective response (22% higher CCB parameter) than the first version.
- Obtaining a higher CCB for the second version of the design proves that the modifications made had a positive effect. Based on the above, the authors conclude that their research method allows not only the effective analysis of the deformation of the UAV, but also the performance of the optimization of its design, aimed at improving the safety of use.

The authors of this paper claim that the development of this measurement system for this research object is possible. This measurement system was created for static-state tests, which can be found as its limitation. To evaluate its nature and impact on structures, e.g. vibrations on structures, full-scale stand tests require this system to be expanded by actuators and vibration sensors as well as a higher frequency DIC system. This aspect seems to be now of the highest potential to develop this system but, importantly, based on the previously created system. The authors claim that the above findings can be considered as solidifying the contribution of this paper to the field's long-term progress. The research object has been implemented into usage and is a testing platform for flights. This fact perfectly confirms that the research was correct and the system that analyzes deformations in such vehicles is practical. The deformation measurement system for UAV components was created for the XGyro project but it is universal and will be applied in the future to examine other unmanned aerial vehicles. The test stand can

be easily modified to suit to other popular unmanned platforms because it is easy to change the spots servo-mechanisms that load a research object and strain gauges to control loading are assembled. The created system is crucial for the planned certification research into UAVs. The application of the system is definitely beneficial for optimizing structures, which confirms its reduced mass. Such improvements mean above all longer flight.

The method described in this paper can be applied to other types of UAVs. The created system is highly applicable. Any number of servos and strain gauges in any configuration can be used on the test stand to simulate loads by real forces due to the operation of the propulsion system of a given aircraft. Aramis system is, on the other hand, a non-contact measurement system, which also means high applicability of the created test stand.

ACKNOWLEDGMENT

This work has been financed by the Polish National Centre for Research and Development under the LIDER program; Grant Agreement No. LIDER/27/0140/L-10/18/NCBR/2019.

REFERENCES

1. Balac M, Grbovic A, Petrovic A, Popovic V. FEM analysis of pressure vessel with an investigation of crack growth on cylindrical surface. Eksploatacja i Niezawodnosc – Maintenance and reliability 2018; 20 (3): 378–386, https://doi.org/10.17531/ein.2018.3.5.
2. Baqersad J, Poozesh P, Niezrecki C, Avitabile P. Photogrammetry and optical methods in structural dynamics – A review. Mechanical Systems and Signal Processing 2017; 86: 17–34, https://doi.org/10.1016/j.ymssp.2016.02.011.
3. Barranco-Gutiérrez A I, Padilla-Medina J A, Perez-Pinal F J, Prado-Olivares J, Martínez-Díaz S, Gutiérrez-Frías O O. New Four Points Initialization for Digital Image Correlation in Metal-Sheet Strain Measurements. Applied Sciences 2019; 9(8): 1691, https://doi.org/10.3390/app9081691.
4. Bleischwitz R, de Kat R, Ganapathisubramani B. Aeromechanics of membrane and rigid wings in and out of ground-effect at moderate Reynolds numbers. Journal of Fluids and Structures 2016; 62: 318–331, https://doi.org/10.1016/j.jfluidstructs.2016.02.005.
5. Borkowski P, Dacko A, Rodzewicz M. Synthesis and Structural Analysis of High Strength Composite Flexible Landing Gear Legs. In Rusiński E, Pietrusiak D (eds): Proceedings of the 13th International Scientific Conference: Computer Aided Engineering, Lecture Notes in Mechanical Engineering. Springer, Cham: 2017, https://doi.org/10.1007/978-3-319-50938-9_6.
6. Bornert M, Hild F, Orteu J J, Roux S. Digital Image Correlation, In: Full-Field Measurements and Identification in Solid Mechanics. Hoboken, NJ, USA, John Wiley & Sons, Inc.: 2012: 157–190, https://doi.org/10.1002/9781118578469.ch6.
7. Chen X, Semenov S, McGugan M, Madsen S H, Yeniceli S C, Berring P, Branner K. Fatigue testing of a 14.3 m composite blade embedded with artificial defects – Damage growth and structural health monitoring. Composites: Part A 2021; 140: 106189, https://doi.org/10.1016/j.compositesa.2020.106189.
8. Curt J, Capaldo M, Hild F, Roux S. Optimal digital color image correlation. Optics and Lasers in Engineering 2020; 127: 105896, https://doi.org/10.1016/j.optlaseng.2019.105896.
9. Dutton S, Kelly D, Baker A. Composite materials for aircraft structures, 2nd edition. AIAA: 2004, https://doi.org/10.2514/4.861680.
10. Flores M, Mollenhauer D, Runatunga V, Beberniss T, Rapking D, Pankow M. High-speed 3D digital image correlation of low-velocity impacts on composite plates. Composites Part B: Engineering 2017; 131: 153–164, https://doi.org/10.1016/j.compositesb.2017.07.078.
11. Gao J X, An Z W, Ma Q, Bai X Z. Residual strength assessment of wind turbine rotor blade composites under combined effects of natural aging and fatigue loads. Eksploatacja i Niezawodnosc – Maintenance and Reliability 2020; 22 (4): 601–609, http://doi.org/10.17531/ein.2020.4.3.
12. Gardner N W, Hilburger M W, Haynie W T, Lindell M C, Waters W A. Digital Image Correlation Data Processing and Analysis Techniques to Enhance Test Data Assessment and Improve Structural Simulations. 2018 AIAA/ASCE/AHS/ASC Structures, Structural Dynamics, and Materials Conference. Kissimmee, Florida, USA, 8-12 January 2018, https://doi.org/10.2514/6.2018-1698.
13. Gradl P R. Digital Image Correlation Techniques Applied to Large Scale Rocket Engine Testing. 52nd AIAA/SAE/ASEE Joint Propulsion Conference. Salt Lake City, Utah, USA, 25-27 July 2016, https://doi.org/10.2514/6.2016-4977.
14. Gu L, Kasavajhala A R M, Zhao S. Finite element analysis of cracks in aging aircraft structures with bonded composite-patch repairs.

Composites Part B: Engineering 2011; 42(3): 505–510, https://doi.org/10.1016/j.compositesb.2010.11.014.
15. Irving P E, Soutis C. Polymer composites in the aerospace industry. Woodhead Publishing: 2014, https://doi.org/10.1016/C2013-0-16303-9.
16. Janeliukstis R, Chen X. Review of digital image correlation application to large-scale composite structure testing. Composite Structures 2021; 271: 114143, https://doi.org/10.1016/j.compstruct.2021.114143.
17. Jebacek I. Measurement of the strain and bending moment on the wing of an aircraft and using of these findings for fatigue test. 27th International Congress of the Aeronautical Sciences. Nice, France, 19-24 September 2010, https://www.icas.org/ICAS_ARCHIVE/ICAS2010/PAPERS/370.PDF.
18. Khadka A, Fick B, Afshar A, Tavakoli M, Baqersad J, Non-contact vibration monitoring of rotating wind turbines using a semi-autonomous UAV. Mechanical Systems and Signal Processing 2020; 138: 106446, https://doi.org/10.1016/j.ymssp.2019.106446.
19. Krawczyk Ł, Gołdyn M, Urban T. About Inaccuracies of DIC System (polish: O Niedokładnościach Systemów Cyfrowej Korelacji Obrazu). Journal of Civil Engineering, Environment and Architecture 2017; t. XXXIV, z. 64 (3/I/17): 259–270, https://doi.org/10.7862/rb.2017.120.
20. Littell J. Large Field Digital Image Correlation Used for Full-Scale Aircraft Crash Testing: Methods and Results. In Sutton M, Reu R L (eds): International Digital Imaging Correlation Society, Conference Proceedings of the Society for Experimental Mechanics Series. Springer, Cham: 2017: 235–239, https://doi.org/10.1007/978-3-319-51439-0_56.
21. Łusiak T, Kneć M. Use of ARAMIS for Fatigue Process Control in the Accelerated Test for Composites. Transportation Research Procedia 2018; 35: 250–258, https://doi.org/10.1016/j.trpro.2018.12.023.
22. Mwelango M, Zhu T, Wen K, Zhang Z, Yuan X, Li W, Yin X. Coplanar capacitive sensors and their applications in non-destructive evaluation: a review. Nondestructive Testing and Evaluation 2023, 1-45. https://doi.org/10.1080/10589759.2023.2198233.
23. Patil K, Srivastava V, Baqersad J. A multi-view optical technique to obtain mode shapes of structures. Measurement 2018; 122: 358–367, https://doi.org/10.1016/j.measurement.2018.02.059.
24. Schreier H, Orteu J J, Sutton M A, Image Correlation for Shape, Motion and Deformation Measurements. Boston, MA, USA, Springer: 2009, https://doi.org/10.1007/978-0-387-78747-3.
25. Shin H G, Timilsina S, Sohn K S, Kim J S. Digital image correlation compatible mechanoluminescent skin for structural health monitoring. Advanced Science 2022, 9(11), 2105889. https://doi.org/10.1002/advs.202105889.
26. Soutis C. Fibre reinforced composites in aircraft construction. Progress in Aerospace Sciences 2005; 41(2): 143–151, https://doi.org/10.1016/j.paerosci.2005.02.004.
27. Splichal J, Pistek A, Hlinka J. Dynamic tests of composite panels of an aircraft wing. Progress in Aerospace Sciences 2015; 78: 50–61, https://doi.org/10.1016/j.paerosci.2015.05.005.
28. Stasicki B, Boden F. In-flight measurements of aircraft propeller deformation by means of an autarkic fast rotating imaging system. International Conference on Experimental Mechanics 2014, Proceedings of SPIE 9302 (2015), 93022S, https://doi.org/10.1117/12.2081393.
29. Tavares S M O, de Castro P M S T. An overview of fatigue in aircraft structures. Special Issue - Fatigue of Aeronautical Materials & Structures 2017; 40(10): 1510–1529, https://doi.org/10.1111/ffe.12631.
30. Wojtas M, Szczepanik T, Czajkowski Ł. New technology of layered structures implemented in selected gyroplane components. 31st Congress of the International Council of the Aeronautical Sciences. Belo Horizonte, Brasil, 9-14 September 2018, https://www.icas.org/ICAS_ARCHIVE/ICAS2018/data/papers/ICAS2018_0356_paper.pdf.
31. Ye M, Liang J, Li L, Qian B, Ren M, Zhang M, Lu W, Zong Y. Full-field motion and deformation measurement of high speed rotation based on temporal phase-locking and 3D-DIC. Optics and Lasers in Engineering 2021; 146: 106697, https://doi.org/10.1016/j.optlaseng.2021.106697.
32. Zhang Z, Mao H, Liu Y, Jia P, Hu W, Shen P. A risk assessment method of aircraft structure damage maintenance interval considering fatigue crack growth and detection rate. Eksploatacja i Niezawodnosc – Maintenance and Reliability 2023: 25(1), http://doi.org/10.17531/ein.2023.1.3.